catalysts

MDPI

Article

Solid Acid Catalyst Based on Single-Layer α-Zirconium Phosphate Nanosheets for Biodiesel Production via Esterification

Yingjie Zhou [1,2,3], Iman Noshadi [3], Hao Ding [3], Jingjing Liu [3], Richard S. Parnas [3], Abraham Clearfield [4], Min Xiao [1], Yuezhong Meng [1,*] and Luyi Sun [3,*]

1 The Key Laboratory of Low-Carbon Chemistry & Energy Conservation of Guangdong Province, State Key Laboratory of Optoelectronic Materials and Technologies, School of Physics and Engineering, Sun Yat-sen University, Guangzhou 510275, China; zyj8703@163.com (Y.Z.); stsxm@mail.sysu.edu.cn (M.X.)
2 Department of Materials Physics, School of Physics and Optoelectronic Engineering, Nanjing University of Information Science & Technology, Nanjing 210044, China
3 Institute of Materials Science and Department of Chemical & Biomolecular Engineering, University of Connecticut, Storrs, CT 06269, USA; noshadi@rowan.edu (I.N.); hao.2.ding@uconn.edu (H.D.); jingjing.liu@uconn.edu (J.L.); richard.parnas@uconn.edu (R.S.P.)
4 Department of Chemistry, Texas A&M University, College Station, TX 77842, USA; clearfield@chem.tamu.edu
* Correspondence: mengyzh@mail.sysu.edu.cn (Y.M.); luyi.sun@uconn.edu (L.S.); Tel.: +86-20-8411-4113 (Y.M.); +860-486-6895 (L.S.); Fax: +86-20-8411-4113 (Y.M.); +860-486-4745 (L.S.)

Received: 21 December 2017; Accepted: 8 January 2018; Published: 10 January 2018

Abstract: In this study, a solid acid was prepared by the sulfonation of surface modified α-zirconium phosphate (ZrP) single-layer nanosheets (SO_3H@ZrP), and the prepared solid acid was investigated for the esterification of oleic acid with methanol to produce biodiesel. For comparison, liquid H_2SO_4 and commercial Amberlyst® 15 catalyst were also evaluated for the same reaction under the same conditions. The experimental results showed that the SO_3H@ZrP solid acid catalyst has a superior catalytic efficiency for the esterification reaction, as well as excellent recyclability. The SO_3H@ZrP single-layer solid acid catalyst can be uniformly dispersed in the reaction media, but remains heterogeneous and thus can be easily separated and recycled.

Keywords: α-zirconium phosphate; solid acid catalyst; single-layer nanosheets; esterification; biodiesel

1. Introduction

In the past decade, biofuels have emerged as an alternative energy source to fossil fuels to relieve the energy crisis and environmental pollution [1,2]. One of the most promising biofuels is biodiesel, which is usually derived from renewable feedstock, such as plant lipids, animal fats/oils, cooking oils/wastes, and inedible oils, etc. [2–4]. The most readily implemented and low-cost route for the synthesis of biodiesel is catalytic esterification and transesterification of free fatty acids (FFAs) [5]. Basic catalysts, including NaOH, KOH, $NaOCH_3$, and $KOCH_3$, are primarily employed [3]. However, these basic catalysts could easily react with fatty acids to form soap, which is unfavorable for the product separation. Likewise, acid catalysts, such as H_2SO_4, HCl, BF_3, and H_3PO_4, are adopted to promote the esterification of FFAs. However, corrosion resistant equipment is required because of the high acidity of the above acid catalysts. In addition, extra separation and neutralization steps generate a large quantity of wastewater. Therefore, the development of heterogeneous acid catalysts are highly desirable to both lower the equipment requirement and minimize the negative impact on the environment.

To date, numerous solid acid catalysts have been developed, including zeolite [6], heteropolyacids [7], ion exchange polymer resins [8–10], carbon-based solid acids [11], and zinc lanthanum mixed oxides [12]. These solid acid catalysts lead to a more facile process and a lower production cost for esterification reactions. However, the limited active sites of these heterogeneous solid acid catalysts prohibit their widespread application. In addition, their relatively low porosity is not favorable for the mass transfer of reactants by diffusion, which leads to a low reaction rate. As a result, the development of solid acid catalysts with a high concentration of acid sites that are easily accessible is highly desired.

α-Zirconium phosphate [ZrP, $Zr(HPO_4)_2 \cdot H_2O$] is a layered compound with a high ion exchange capacity, which can be exfoliated into single-layer nanosheets [13]. The crystallinity and size of ZrP can be controlled by varying the synthetic conditions [14–16]. Therefore, ZrP has been widely applied in constructing versatile functional materials, such as catalysts [17–20], polymer nanocomposites [21–28], and intercalation compounds [23,29–31], etc. The unique structure of ZrP allows it to be an excellent support for the anchoring of functional groups. Moreover, the exfoliated ZrP single-layer nanosheets can be readily and uniformly dispersed in a reaction system, which allows for a high accessibility of the functional groups.

In this work, the solid acid catalyst based on sulfonic acid functionalized ZrP single-layer nanosheets was applied as a catalyst for the esterification of oleic acid with methanol. The solid acid exhibited comparable catalytic activity to liquid H_2SO_4, and even higher activity than the commercial Amberlyst® 15.

2. Results and Discussion

The procedures for the preparation of SO_3H@ZrP are illustrated in Figure 1. The pristine ZrP (Figure 2a) was exhibited as hexagonal crystal discs with an average lateral dimension of ca. 450 nm, and Figure 2b shows the size distribution of the discs. The micro-crystals were exfoliated by TBA to form individual single-layer nanosheets (Figure 2c) [29,32]. Because of the ultrasonication treatment, the single-layer nanosheets were broken down into smaller pieces, with an average lateral dimension of ca. 66 nm (Figure 2d). After grafting γ-propyl mercaptotrimethoxysilane onto the nanosheet surface and the subsequent oxidation to form SO_3H@ZrP, the ZrP host maintained a sheet structure (Figure 2e). The $-SO_3H$ groups could interact with water molecules to form hydrogen bonds, which facilitated the re-stacking of SO_3H@ZrP nanosheets during drying (Figure 2e). Note that the morphology shown in Figure 2e only represents the state of SO_3H@ZrP nanosheets in the solid phase. When SO_3H@ZrP nanosheets are dispersed in the liquid reaction system (a mixture of oleic acid and methanol), one can clearly observe the Tyndall effect (Figure 2f), suggesting that SO_3H@ZrP nanosheets could be uniformly dispersed to form a homogeneous dispersion. Meanwhile, SO_3H@ZrP nanosheets can be easily separated from the dispersion via centrifugation, exhibiting advantages of both homogeneous and heterogeneous catalysts.

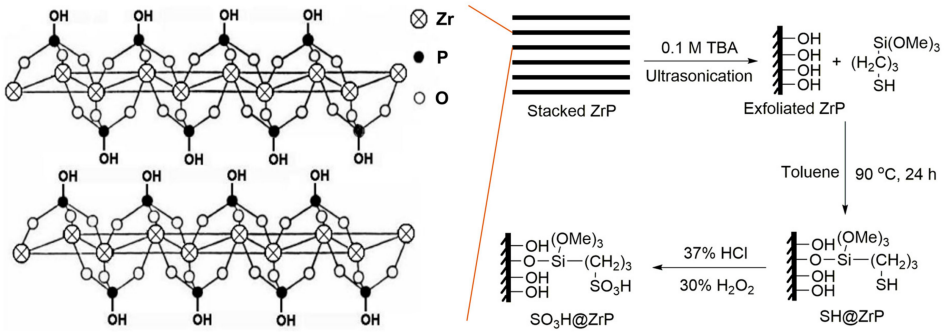

Figure 1. Structure of ZrP and synthesis procedures of SO_3H@ZrP.

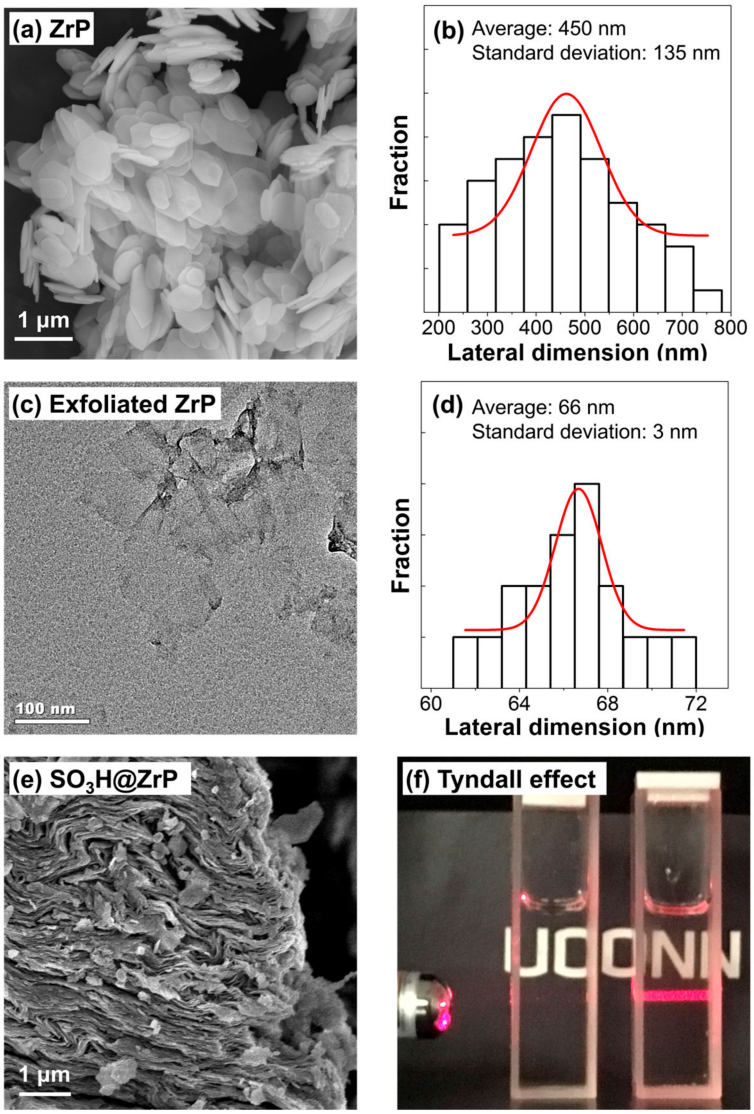

Figure 2. (**a**) SEM image and (**b**) size distribution of the ZrP micro-crystals, (**c**) TEM image and (**d**) size distribution of the exfoliated ZrP single-layer nanosheets, (**e**) SEM image of SO_3H@ZrP, (**f**) the Tyndall effect of SO_3H@ZrP dispersed in the mixture of oleic acid and methanol; the left one is the control sample without SO_3H@ZrP.

In order to verify the grafting of functional groups onto the ZrP sheet surface, FTIR characterization was performed, and the spectra are shown in Figure 3. After the reaction with γ-propyl mercaptotrimethoxysilane, the two peaks at 3512 and 3595 cm^{-1} ascribed to the interlayer molecular water and the out-of-plane vibration of the P–OH groups of ZrP at 970 cm^{-1} vanished [18,29]. Meanwhile, the characteristic absorption peak of –SH located at ca. 2558 $cm^{-1,}$ and methyl groups located in the range of 2834–3020 cm^{-1} could be observed. These changes confirmed the successful grafting of –SH groups onto ZrP nanosheets. After oxidation, the peak belonging to –SH disappeared. Instead, a new peak located at ca. 1195 cm^{-1} assigned to S=O appeared, suggesting that the –SH groups were successfully oxidized into $–SO_3H$ groups.

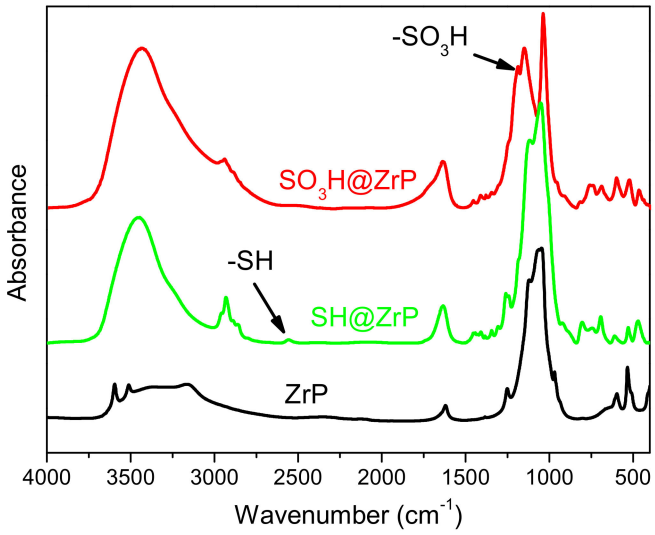

Figure 3. FTIR spectra of the pristine ZrP, SH@ZrP, and SO_3H@ZrP.

The esterification reaction results of oleic acid with methanol catalyzed by SO_3H@ZrP, H_2SO_4, and Amberlyst® 15 are shown in Figure 4. The conversion increased steadily, and gradually slowed down and plateaued for each catalyzed reaction. Liquid H_2SO_4 exhibited the highest catalytic activity of virtually 100% oleic conversion. The catalytic activity of SO_3H@ZrP solid acid is slightly lower, which resulted in a ca. 89% conversion rate after 5 h of reaction. The slightly lower catalytic activity of SO_3H@ZrP in comparison to liquid H_2SO_4 is expected, as liquid H_2SO_4 exhibits the highest possible miscibility and accessibility, as well as a much higher mole amount of functional $–SO_3H$ per unit mass, while in SO_3H@ZrP, the $–SO_3H$ groups are supported on ZrP nanosheets. However, SO_3H@ZrP exhibited higher catalytic activity than the commercial Amberlyst® 15 catalyst, one of the most popular commercial solid acid catalysts. This can be ascribed to the high density of the sulfonic acid groups on the surface of ZrP nanosheets, and their high dispersion and thus high accessibility in the reaction system.

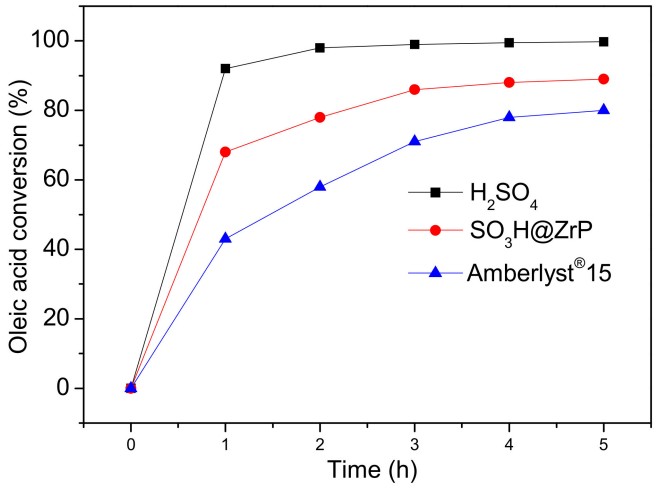

Figure 4. Catalytic activity of SO_3H@ZrP on the esterification of oleic acid with methanol.

While liquid H_2SO_4 exhibited the highest catalytic activity, its liquid nature prohibited effective separation after the completion of the reaction. This is a major issue for its commercial applications. In contrast, solid acid catalysts such as SO_3H@ZrP and Amberlyst® 15 can be easily separated from the reaction system via simple centrifugation and reused for the next reaction.

The recyclability of SO_3H@ZrP solid acid in the esterification of oleic acid with methanol is shown in Figure 5. There is a loss of ca. 9% in the conversion rate after five cycles of reaction, and a loss of ca. 25% in the conversion rate after seven cycles. During catalyst recovery using centrifuge, a trace amount of catalyst was attached to the centrifuge tube, which did not participate in the next catalytic run. So the loss of catalytic activity is believed to be due to the leaching of catalyst during separation at a lab scale, which can be minimized on a large industry scale, rather than from the deactivation of the functional groups. Note that after each cycle of reaction, the SO_3H@ZrP solid acid catalyst was simply washed with CH_2Cl_2 to prepare for the next cycle, but no attempt to regenerate the catalyst was made.

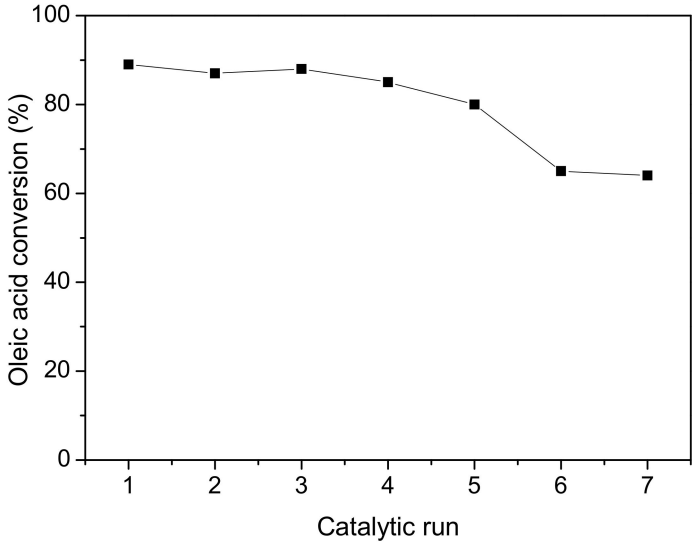

Figure 5. Recyclability of SO_3H@ZrP.

3. Conclusions

In summary, the SO_3H@ZrP solid acid was prepared by the surface modification of ZrP single-layer nanosheets and was evaluated as a solid catalyst for the esterification of oleic acid with methanol. The SO_3H@ZrP solid acid catalyst exhibited higher catalytic activity than the commercial Amberlyst® 15. An oleic acid conversion rate of 89% was achieved, and the solid acid also exhibited a high recyclability. As such, the SO_3H@ZrP solid acid based on single-layer ZrP nanosheets is a promising solid acid catalyst for acid catalyzed reactions.

4. Experimental

4.1. Materials

γ-Propyl mercaptotrimethoxysilane (MPTMS, 95%, Sigma-Aldrich, Saint Louis, MO, USA), hydrogen peroxide (H_2O_2, 30 wt%, Fisher Scientific, Hampton, VA, USA), zirconyl chloride octahydrate ($ZrOCl_2 \cdot 8H_2O$, 98%, Sigma-Aldrich, Saint Louis, MO, USA), phosphoric acid (85%, Sigma-Aldrich, Saint Louis, MO, USA), tetra-*n*-butylammonium hydroxide (TBA, 0.10 M, Sigma-Aldrich, Saint Louis, MO, USA), dichloromethane (CH_2Cl_2, ≥99.5%, Sigma-Aldrich, Saint Louis, MO, USA), methanol (99%, Alfa Aesar, Haverhill, MA, USA), and oleic acid (OA, ≥99%, Sigma-Aldrich, Saint Louis, MO, USA) were used as received without further purification. Common chemicals including sulfonic acid (98 wt%), hydrochloric acid (37 wt%), ethanol, toluene, and acetone were obtained from commercial vendors and used as received. Amberlyst® 15 was purchased from Sigma-Aldrich.

4.2. Preparation of ZrP Nanosheets

ZrP microcrystals were first synthesized by a hydrothermal reaction of $ZrOCl_2 \cdot 8H_2O$ with 6.0 M H_3PO_4 at 200 °C for 24 h in a sealed Teflon-lined pressure vessel according to a reported method [18]. Then, 0.10 M TBA (3.3 mL) was added to 0.10 g of the synthesized ZrP microcrystals dispersed in 6.7 mL H_2O, followed by ultrasonication in an ice bath for 15 min to exfoliate ZrP [29,32]. Subsequently, 0.10 M HCl (3.3 mL) was added into the above mixture to protonate the TBA exfoliated ZrP single-layer nanosheets [27]. The thickness of each ZrP single-layer nanosheet was circa 6.3 Å [33,34].

The protonated ZrP nanosheets were further washed with copious water to eliminate chloride ions, and the obtained gel-like ZrP nanosheets were then rinsed with acetone three times. Subsequently, the gel-like ZrP nanosheets dispersed in acetone were washed by toluene and centrifuged to exchange the solvent from acetone to toluene. The final ZrP nanosheets dispersed in toluene were ready for the immobilization of thiol groups.

4.3. Preparation and Characterization of Solid Acid

A sample of 75 mmol γ-propyl mercaptotrimethoxysilane was mixed with 0.90 g ZrP nanosheets dispersed in 300 mL toluene, and the mixture was refluxed at 90 °C for 24 h under N_2 atmosphere with constant stirring to obtain thiol group grafted ZrP nanosheets (SH@ZrP) [18]. The obtained SH@ZrP sample was washed with toluene, centrifuged, and dried. At the last step, 0.60 g SH@ZrP was dispersed in 24 mL methanol with the assistance of ultrasonication, followed by the addition of 11.0 mL H_2O_2 (30 wt%). The above mixture was aged for 24 h with constant stirring. After that, 10.0 mL HCl (37 wt%) was added to ensure complete oxidation and protonation of the thiol groups. The obtained sample was washed with abundant water and centrifuged until the supernatant was neutral. After being dried, sulfonic acid functionalized ZrP nanosheets (SO_3H@ZrP) were obtained.

The morphology of the samples was characterized by an FEI Helios NanoLab^{TM} 400 DualBeam^{TM} scanning electron microscope (SEM) (FEI Company, Hillsboro, OR, USA) and a JEOL 2010F field-emission transmission electron microscopy (TEM) (JEOL Ltd., Tokyo, Japan). The Fourier transform infrared spectroscopy (FTIR) (Analect LLC, Huntington, NY, USA) spectra of the samples were recorded on an Analect RFX-65A FTIR spectrophotometer.

4.4. Esterification of Oleic Acid with Methanol

Esterification of oleic acid was carried out under the catalysis of SO_3H@ZrP at 65 °C in a flask fitted with a water-cooled reflux condenser. For comparison, liquid H_2SO_4 and commercial Amberlyst® 15 were also evaluated as alternative catalysts. The mole ratio of methanol to oleic acid was maintained at 9:1. All of the catalysts were used at the same mass concentration, 5.0% (*w*/*w*), with respect to oleic acid. The samples collected periodically were centrifuged to form two layers: the upper layer being water and methanol, and the bottom layer being methyl esters of oleic acid. The bottom layer was titrated to determine the amount of remaining oleic acid to calculate the rate of conversion. After each reaction, the SO_3H@ZrP catalyst was recycled by centrifugation and washed with CH_2Cl_2 for the next catalytic run.

Acknowledgments: We gratefully acknowledge the financial support from the ACS Petroleum Research Fund (Grant No. 57580-ND5) and the National Science Foundation (CMMI-1562907).

Author Contributions: Luyi Sun and Yuezhong Meng conceived and designed the experiments. Yingjie Zhou, Iman Noshadi, Hao Ding, and Jingjing Liu performed the experiments and analyzed the data. Richard S. Parnas, Abraham Clearfield, and Min Xiao discussed the experiments and data in this work. Luyi Sun, Yingjie Zhou, and Richard S. Parnas wrote the manuscript. All authors discussed the results and commented on the manuscript.

Conflicts of Interest: The authors declare no conflict of interest.

References

1. Su, F.; Guo, Y. Advancements in solid acid catalysts for biodiesel production. *Green Chem.* **2014**, *16*, 2934–2957. [CrossRef]
2. Lee, A.F.; Bennett, J.A.; Manayil, J.C.; Wilson, K. Heterogeneous catalysis for sustainable biodiesel production via esterification and transesterification. *Chem. Soc. Rev.* **2014**, *43*, 7887–7916. [CrossRef] [PubMed]
3. Melero, J.A.; Iglesias, J.; Morales, G. Heterogeneous acid catalysts for biodiesel production: Current status and future challenges. *Green Chem.* **2009**, *11*, 1285–1308. [CrossRef]
4. Noshadi, I.; Kanjilal, B.; Du, S.; Bollas, G.M.; Suib, S.L.; Provatas, A.; Liu, F.; Parnas, R.S. Catalyzed production of biodiesel and bio-chemicals from brown grease using Ionic Liquid functionalized ordered mesoporous polymer. *Appl. Energy* **2014**, *129*, 112–122. [CrossRef]
5. Talebian-Kiakalaieh, A.; Amin, N.A.S.; Mazaheri, H. A review on novel processes of biodiesel production from waste cooking oil. *Appl. Energy* **2013**, *104*, 683–710. [CrossRef]
6. Chung, K.-H.; Park, B.-G. Esterification of oleic acid in soybean oil on zeolite catalysts with different acidity. *J. Ind. Eng. Chem.* **2009**, *15*, 388–392. [CrossRef]
7. Shin, H.Y.; An, S.H.; Sheikh, R.; Park, Y.H.; Bae, S.-H. Transesterification of used vegetable oils with a Cs-doped heteropolyacid catalyst in supercritical methanol. *Fuel* **2012**, *96*, 572–578. [CrossRef]
8. Pan, Y.; Alam, M.A.; Wang, Z.; Wu, J.; Zhang, Y.; Yuan, Z. Enhanced esterification of oleic acid and methanol by deep eutectic solvent assisted Amberlyst heterogeneous catalyst. *Bioresour. Technol.* **2016**, *220*, 543–548. [CrossRef] [PubMed]
9. Ilgen, O. Investigation of reaction parameters, kinetics and mechanism of oleic acid esterification with methanol by using Amberlyst 46 as a catalyst. *Fuel Process. Technol.* **2014**, *124*, 134–139. [CrossRef]
10. Reis, S.C.M.D.; Lachter, E.R.; Nascimento, R.S.V.; Rodrigues, J.A.; Reid, M.G. Transesterification of Brazilian vegetable oils with methanol over ion-exchange resins. *J. Am. Oil Chem. Soc.* **2005**, *82*, 661–665. [CrossRef]
11. Liu, T.; Li, Z.; Li, W.; Shi, C.; Wang, Y. Preparation and characterization of biomass carbon-based solid acid catalyst for the esterification of oleic acid with methanol. *Bioresour. Technol.* **2013**, *133*, 618–621. [CrossRef] [PubMed]
12. Yan, S.; Salley, S.O.; Ng, K.S. Simultaneous transesterification and esterification of unrefined or waste oils over ZnO-La_2O_3 catalysts. *Appl. Catal. Gen.* **2009**, *353*, 203–212. [CrossRef]
13. Sun, L.; Boo, W.J.; Sun, D.; Clearfield, A.; Sue, H.-J. Preparation of exfoliated epoxy/α-zirconium phosphate nanocomposites containing high aspect ratio nanoplatelets. *Chem. Mater.* **2007**, *19*, 1749–1754. [CrossRef]
14. Sun, L.; Boo, W.J.; Sue, H.-J.; Clearfield, A. Preparation of α-zirconium phosphate nanoplatelets with wide variations in aspect ratios. *New J. Chem.* **2007**, *31*, 39–43. [CrossRef]
15. Pica, M.; Donnadio, A.; Capitani, D.; Vivani, R.; Troni, E.; Casciola, M. Advances in the chemistry of nanosized zirconium phosphates: A new mild and quick route to the synthesis of nanocrystals. *Inorg. Chem.* **2011**, *50*, 11623–11630. [CrossRef] [PubMed]
16. Pica, M.; Donnadio, A.; Mariangeloni, G.; Zuccaccia, C.; Casciola, M. A combined strategy for the synthesis of double functionalized α-zirconium phosphate organic derivatives. *New J. Chem.* **2016**, *40*, 8390–8396. [CrossRef]
17. Pica, M.; Nocchetti, M.; Ridolfi, B.; Donnadio, A.; Costantino, F.; Gentili, P.L.; Casciola, M. Nanosized zirconium phosphate/AgCl composite materials: A new synergy for efficient photocatalytic degradation of organic dye pollutants. *J. Mater. Chem. A* **2015**, *3*, 5525–5534. [CrossRef]
18. Zhou, Y.; Huang, R.; Ding, F.; Brittain, A.D.; Liu, J.; Zhang, M.; Xiao, M.; Meng, Y.; Sun, L. Sulfonic acid-functionalized α-zirconium phosphate single-layer nanosheets as a strong solid acid for heterogeneous catalysis applications. *ACS Appl. Mater. Interfaces* **2014**, *6*, 7417–7425. [CrossRef] [PubMed]
19. Zhou, Y.; Wang, A.; Wang, Z.; Chen, M.; Wang, W.; Sun, L.; Liu, X. Titanium functionalized α-zirconium phosphate single layer nanosheets for photocatalyst applications. *RSC Adv.* **2015**, *5*, 93969–93978. [CrossRef]
20. Zhou, Y.; Liu, J.; Huang, R.; Zhang, M.; Xiao, M.; Meng, Y.; Sun, L. Covalently immobilized ionic liquids on single layer nanosheets for heterogeneous catalysis applications. *Dalton Trans.* **2017**, *46*, 13126–13134. [CrossRef] [PubMed]
21. Pica, M.; Donnadio, A.; Casciola, M. Starch/zirconium phosphate composite films: Hydration, thermal stability, and mechanical properties. *Starch-Stärke* **2012**, *64*, 237–245. [CrossRef]

22. Casciola, M.; Alberti, G.; Donnadio, A.; Pica, M.; Marmottini, F.; Bottino, A.; Piaggio, P. Gels of zirconium phosphate in organic solvents and their use for the preparation of polymeric nanocomposites. *J. Mater. Chem.* **2005**, *15*, 4262–4267. [CrossRef]
23. Boo, W.J.; Sun, L.; Liu, J.; Clearfield, A.; Sue, H.-J. Effective intercalation and exfoliation of nanoplatelets in epoxy via creation of porous pathways. *J. Phys. Chem. C* **2007**, *111*, 10377–10381. [CrossRef]
24. Sun, L.; Boo, W.J.; Browning, R.L.; Sue, H.-J.; Clearfield, A. Effect of Crystallinity on the Intercalation of Monoamine in α-Zirconium Phosphate Layer Structure. *Chem. Mater.* **2005**, *17*, 5606–5609. [CrossRef]
25. Pica, M.; Donnadio, A.; Troni, E.; Capitani, D.; Casciola, M. Looking for New Hybrid Polymer Fillers: Synthesis of Nanosized α-Type Zr(IV) Organophosphonates through an Unconventional Topotactic Anion Exchange Reaction. *Inorg. Chem.* **2013**, *52*, 7680–7687. [CrossRef] [PubMed]
26. Boo, W.J.; Sun, L.; Liu, J.; Clearfield, A.; Sue, H.-J.; Mullins, M.J.; Pham, H. Morphology and mechanical behavior of exfoliated epoxy/α-zirconium phosphate nanocomposites. *Comp. Sci. Tech.* **2007**, *67*, 262–269. [CrossRef]
27. Sun, L.; Boo, W.-J.; Clearfield, A.; Sue, H.-J.; Pham, H.Q. Barrier properties of model epoxy nanocomposites. *J. Membr. Sci.* **2008**, *318*, 129–136. [CrossRef]
28. Sun, L.; Liu, J.; Kirumakki, S.R.; Schwerdtfeger, E.D.; Howell, R.J.; Al-Bahily, K.; Miller, S.A.; Clearfield, A.; Sue, H.-J. Polypropylene nanocomposites based on designed synthetic nanoplatelets. *Chem. Mater.* **2009**, *21*, 1154–1161. [CrossRef]
29. Zhou, Y.; Liu, J.; Xiao, M.; Meng, Y.; Sun, L. Designing Supported Ionic Liquids (ILs) within Inorganic Nanosheets for CO_2 Capture Applications. *ACS Appl. Mater. Interfaces* **2016**, *8*, 5547–5555. [CrossRef] [PubMed]
30. Lu, N.; Lin, K.-Y.; Kung, C.-C.; Jhuo, J.-W.; Zhou, Y.; Liu, J.; Sun, L. Intercalated polyfluorinated Pd complexes in α-zirconium phosphate for Sonogashira and Heck reactions. *RSC Adv.* **2014**, *4*, 27329–27336. [CrossRef]
31. Hu, H.; Martin, J.C.; Xiao, M.; Southworth, C.S.; Meng, Y.; Sun, L. Immobilization of ionic liquids in layered compounds via mechanochemical intercalation. *J. Phys. Chem. C* **2011**, *115*, 5509–5514. [CrossRef]
32. Kaschak, D.M.; Johnson, S.A.; Hooks, D.E.; Kim, H.-N.; Ward, M.D.; Mallouk, T.E. Chemistry on the edge: A microscopic analysis of the intercalation, exfoliation, edge functionalization, and monolayer surface tiling reactions of α-zirconium phosphate. *J. Am. Chem. Soc.* **1998**, *120*, 10887–10894. [CrossRef]
33. Alberti, G. Syntheses, crystalline structure, and ion-exchange properties of insoluble acid salts of tetravalent metals and their salt forms. *Acc. Chem. Res.* **1978**, *11*, 163–170. [CrossRef]
34. Alberti, G.; Casciola, M.; Costantino, U. Inorganic ion-exchange pellicles obtained by delamination of α-zirconium phosphate crystals. *J. Colloid Interface Sci.* **1985**, *107*, 256–263. [CrossRef]